lubricants

MDPI

Article

Carbonaceous Decomposition Products at High Temperatures and Their Interfacial Role in the Friction Behaviour of Composite Brake Material

Piyush Chandra Verma [1,*], Pranesh Aswath [2], Giovanni Straffelini [3] and Stefano Gialanella [3]

[1] Department of Mechanical Engineering, Birla Institute of Technology and Science, Pilani, Hyderabad Campus, Telangana 500078, India
[2] College of Engineering, University of Texas at Arlington, Arlington, TX 76019, USA; aswath@exchange.uta.edu
[3] Dipartimento di Ingegneria Industriale, Università di Trento, Via Sommarive 9, Povo, 38123 Trento, Italy; giovanni.straffelini@unitn.it (G.S.); stefano.gialanella@unitn.it (S.G.)
* Correspondence: piyushchandraverma@hyderabad.bits-pilani.ac.in

Abstract: This study aims to investigate the outcomes of carbonaceous products, derived from the decomposition of the components of vehicular brake materials, under high-temperature wear tests. Pin-on-disc (PoD) wear tests were conducted by using cast iron discs against pins made of commercially available low-steel friction material. Tests were carried out at different temperatures: 155 °C, 200 °C, 250 °C, and 300 °C. The characterization of the sliding plateaus on worn pin surfaces was based on X-ray diffraction (XRD), scanning electron microscopy (SEM), and Raman spectroscopy. It was noted that at temperatures above 200 °C, the thermal degradation of the inorganic resin, used as a material binder, occurs. An interesting observation was recorded at 300 °C; the brake pin material's friction curve showed higher stability despite having an excessive wear rate. However, the brake pin's specific wear coefficient was higher at this temperature than was observed in the other friction tests. A detailed study of the friction plateaus on the worn-out pins at 300 °C revealed that the decomposed carbon resin product, i.e., the distorted graphite, was widespread over the surface of the pin. Lubricant stabilization can be expected, as established by the observed values of the coefficient of friction (CoF), retaining values within the 0.4–0.6 range, even at high temperatures. Other friction material components may have contributed to the formation of this ubiquitous carbonaceous interface film.

Keywords: pin-on-disc; friction film; Raman spectroscopy; powder diffraction; SEM; high-temperature wear test

Citation: Verma, P.C.; Aswath, P.; Straffelini, G.; Gialanella, S. Carbonaceous Decomposition Products at High Temperatures and Their Interfacial Role in the Friction Behaviour of Composite Brake Material. *Lubricants* **2024**, *12*, 399. https://doi.org/10.3390/lubricants12110399

Received: 27 September 2024
Revised: 14 November 2024
Accepted: 18 November 2024
Published: 20 November 2024

1. Introduction

Brake pads are made of highly complex composite materials and play a vital role in stopping the vehicle during regular or emergency braking. The primary safety challenge in the automotive braking system is the variation in the coefficient of friction (CoF) between the contact surfaces. The consequence of variation in the CoF leads to an extended stopping distance after braking, with evident safety consequences.

The primary constituents that control the brake pad's performance include friction additives, fillers, reinforcement fibres, and binders, [1–4], among which the role of the binder in high-temperature friction testing is the subject of investigation [5–7]. During braking, the brake pads undergo relative interactions with their rotor counterpart, releasing a significant amount of wear debris from both mating surfaces. Part of this product goes into the atmosphere, with a hazardous environmental impact [8–15]. In the braking process, the sliding surfaces trap some wear debris to form a friction layer through a combination of load compaction and temperature sintering [16]. This friction film characterizes the brake pad wear pattern seen in sliding contact.

Consistent coefficients of friction and low wear rates have been observed as long as the friction films on the sliding surfaces are not damaged by abrasive wear particles from sliding bodies. The formation of primary and secondary plateaus is a result of a continuously repeated process that leads to the creation and disruption of the friction layers. Primary plateaus are composed of large, hard particles and tough metallic and non-metallic reinforcing fibres, while secondary plateaus are formed by compacting and sintering the wear debris accumulated by the primary plateaus. Consequently, the friction and wear behaviour of the brake pad–disc system is influenced by the development of the friction film, which is determined by the compactness and thickness of the film. If this friction film delaminates, a significant amount of wear debris and fragments will be released.

Temperature impacts the wear rate and friction behaviour of the sliding system. Phenolic resins, commonly used as binders, may decompose at high working temperatures. This can lead to an increase in wear rate and an unstable friction coefficient, due to the formation of a discontinuous friction film [17]. Phenolic resins, which are naturally thermosetting, affect the wear and friction behaviour of the sliding system when they decompose at high operating temperatures.

The components and resulting microstructure of a brake pad material play a significant role in the relevant friction and wear behaviour seen at high temperatures, resulting from frequent and intense braking actions. The choice of ingredients becomes vital to provide a steady coefficient of friction and lower wear rate at high temperatures and under extreme braking conditions.

In this context, P.C. Verma et al. [18] used a pin-on-disc tribometer, in which the discs were kept at various high temperatures to demonstrate the tribological behaviour of a commercial friction material used for brake pads. Because the binder resin in the pin material thermally decomposed at a high temperature, i.e., 300 °C, a severe wear regime was examined.

This study investigates the influence of temperature on the tribological behaviour of a commercial low-steel friction material when dry sliding against a cast iron disc. A high-temperature pin-on-disc wear test rig was used, specifically at 155 °C, 200 °C, 250 °C, and 300 °C, and we maintained a constant load and sliding speed for all the high-temperature friction tests.

The aim of this research is to better understand the tribological phenomena occurring at the friction pair interface, particularly the processes behind the significant growth of the CoF curve, which is accompanied by an excessive wear rate at high temperatures. To achieve this goal, we used the X-ray diffraction (XRD) technique to analyze the worn-out surfaces of the tested pins. The quantitative evaluation of the different phases was conducted using full-pattern fitting of Rietveld analysis. Raman spectroscopy and scanning electron microscope (SEM) observations were used to characterize the worn-out pin surfaces.

2. Experimental Details

2.1. Friction Material

In this investigation, a Grey Cast Iron (GCI) disc with a hardness of 350 ± 11 HV60 was used as a rotor, and a commercial low-steel friction material was chosen for the pins. The actual cylindrical pin, measuring 5.5 ± 0.2 mm in diameter and 7.5 ± 0.5 mm in height, can be seen in Figure 1a after being removed from the commercial brake pad by water jet machining. The density of the brake pin material was 1.91 g/cm^3. The main phases identified in the virgin brake material are listed in Table 1a,b and were calculated from XRF spectroscopy data with the assistance of stoichiometry. The distribution of hard abrasive magnesium oxide is shown in Figure 1b: Dark black phases are labelled as “B” and steel fibre is labelled as “A”. The area denoted as “C” is rich in tin and sulphur, while “D” is rich in Fe, Mg, Ca, and Zn.

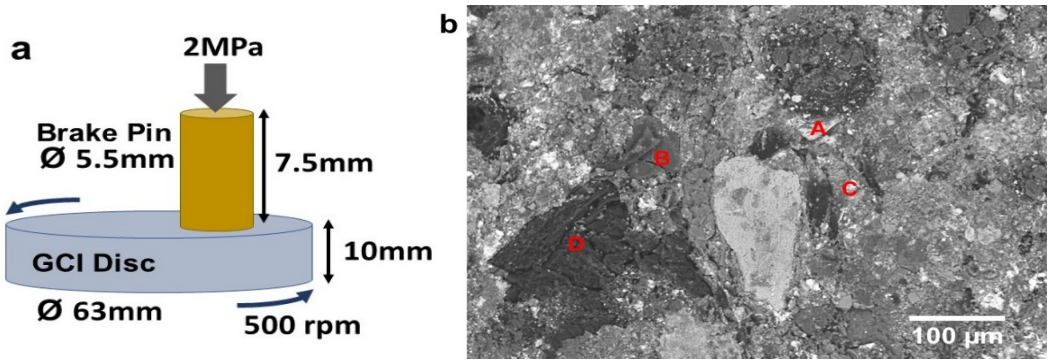

Figure 1. (**a**) Cylindrical shape brake material pin placed on GCI disc. (**b**) Microstructure of virgin brake material.

Table 1. (a) X-ray fluorescence spectroscopy (XRF) elemental composition of brake material. (b) A list of various compound stoichiometries present in the brake material.

(a) Elements	Zn	Mg	Al	Sn	Fe	Si	Cu	S	Ca	Cr	K	Ti	Zr	P	Bal
Wt %	12.5	10.4	9.1	8.7	7.1	5.8	5.4	5.2	5.0	3.6	0.6	0.2	0.05	0.05	ND
(b) Components	Magnesium oxide (MgO)		Tin Sulphide (SnS)		Alumina (Al_2O_3)		Vermiculite $(Mg,Fe^{2+},Fe^{3+})_3[(Al,Si)_4O_{10}]$		Zinc Oxide (ZnO)		Calcium Phosphate ($Ca_3P_2O_8$)		Pyrite (FeS)	Graphite fibres, organic resin, and carbon	
Wt %	14.1		9.3		5.7		13.6		13.8		2.8		9.4	Bal.	

The primary elemental components of the friction material were determined using an X-ray fluorescence (XRF) probe, and the composition is given in Table 1.

2.2. High-Temperature Pin-on-Disc Test Setup

The pin-on-disc friction tests were carried out in a high-temperature tribometer configuration created in the lab. The high-temperature closed-loop feedback friction test system is shown in Figure 2.

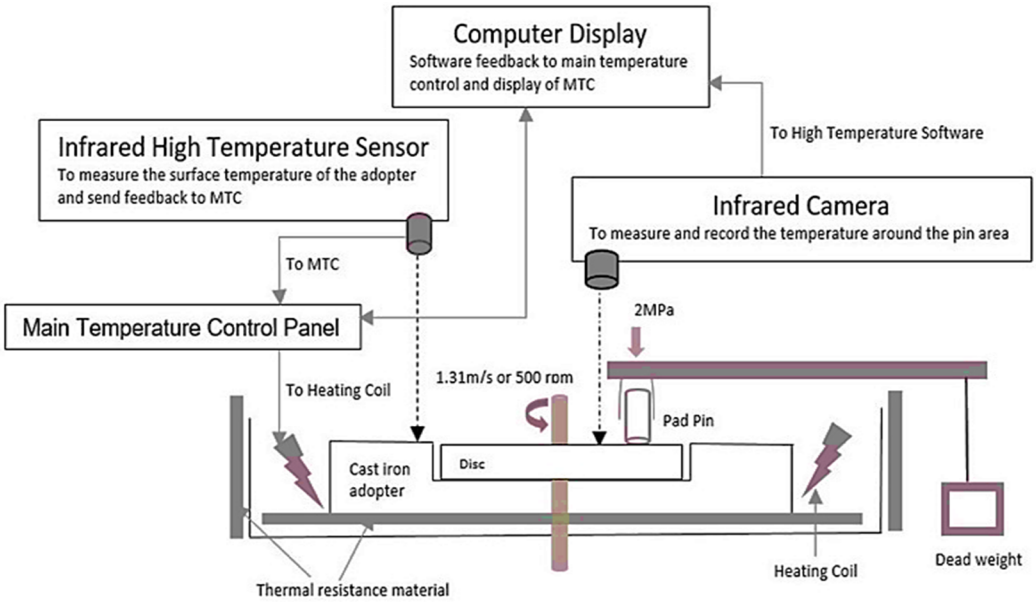

Figure 2. High-temperature wear test rig.

The heating coil in the closed-loop feedback system was further tuned by a primary temperature control panel linked to an infrared high-temperature sensor and camera, maintaining the temperature of the cast iron disc at the set test value. The test was conducted

at various disc temperatures—namely, 155 °C, 200 °C, 250 °C, and 300 °C—to investigate the impact of the wear products, including the carbonaceous components deriving from the degradation of the binder, on the tribological behaviour of the pin–disc system. A 63 mm cast iron disc was inserted into the circular groove of a 140 mm cast iron adopter to obtain a more characterization-appropriate fit. The top surface of the cast iron adopter was painted with high-emissivity black paint to reduce the amount of infrared radiation reflected from the cast iron metallic surface. The disc and adapter geometries were checked for any clearance. If they persisted, the clearance was filled with thermally conductive paste to ensure adequate thermal coupling. Furthermore, to enhance the safety feature, the entire pin-on-disc test rig area near the adopter was wrapped with refractory alumina for adequate thermal insulation and to protect the nearby gears and electric motors within the test rig.

The removed brake pins were rubbed on the bottom side, opposite the test surface, using SiC 800 grit abrasive paper before the high-temperature friction test to obtain better thermal contact with the pin holder and conformal contact with the disc. Each test had operating circumstances with a linear speed of 1.31 m/s, corresponding to the disc's rotating speed (500 RPM). A standard load of 2 MPa was applied, and the total sliding distance was 4000 m. Each test lasted 50 min. The pin's wear was assessed after each friction test using the pin's weight before and after the test. This was performed using an analytical balance with an accuracy of 10^{-4} g. The relationships in Equations (1) and (2) were used to calculate the total wear volume (V) and specific wear volume (W), respectively.

$$\text{Total Wear Volume } (V) = (W_b - W_a)/\rho \quad (1)$$

$$\text{Specific Wear Volume } (W) = (W_b - W_a)/\rho d \quad (2)$$

W_b and W_a represent the pin's weight before and after each friction test. The sliding distance is denoted by "d", while the pin material's density is given by "ρ". The specific wear coefficient, which is symbolized by the letter "Ka" and may be calculated from total wear volume, can be found in Equation (3).

$$Ka = W/Fd \quad (3)$$

where F stands for the normal force applied.

Three high-temperature friction tests were carried out to analyze mean friction and specific wear rate data to obtain statistically and repeatable friction data with an error not exceeding 5%.

2.3. Characterization Tools

To identify the crystalline phases of the friction film, X-ray diffraction measurements were performed using an IPD 3000 Diffractometer (compact 3K5 X-ray generator, CuK_α (λ = 1.5406 Å) radiation with a Ni-filter). The X-ray generator was set at 40 kV and 30 mA.

The virgin brake pad pin's microstructure and worn-out pin planner surfaces were examined using a scanning electron microscope (SEM). The composition of the friction plateaus was examined using an energy-dispersive X-ray spectroscopy (EDXS) system, attached to the SEM. A 3D optical profilometer was used to assess the wear track profile on the cast iron disc.

A Raman spectrometer (Thermo Scientific DXR spectrometer, Thermo Fisher Scientific, Waltham, MA, USA) was utilized to study the friction plateaus, particularly the decomposed resin, using a diode-pumped solid-state laser. The collecting system was selected as a back-dispersed design. The materials were inspected by gazing at them via a low-mag microscope objective lens without any sample preparation. The spectra were obtained at the three areas with most sediments. The regions were inspected with a microscope prior to the spectra measurement. The average spectra were obtained by averaging the intensity values at each Raman shift (frequency) across all the individual spectra. The

Raman spectra were recorded using a solid-state laser with a maximum output of 10 mW and a wavelength of 532 nm. The low laser power was necessary to prevent the sample from overheating. The diameter of the entirely focused laser beam was 2 μm, and the slit width was 25 mm. The spectral resolution at 532 nm was 5 cm^{-1}, with a wavelength range of 50 cm^{-1} to 3500 cm^{-1}. Each measurement was performed over 10 scans, and the total acquisition time amounted to 15 min.

3. Results and Discussion

3.1. The Evolution of Friction and Wear with Test Temperature

Figure 3 shows the outcomes of tests employing brake pad pin material sliding on a cast iron disc at different temperatures. The temperature dependence of the frictional behaviour of the friction materials is shown in Table 2.

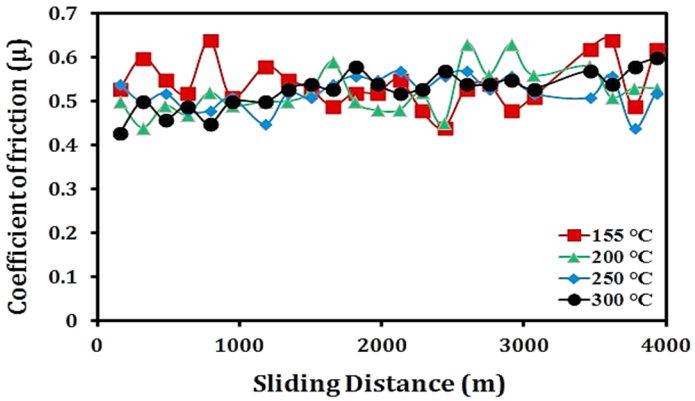

Figure 3. The evolution of the friction coefficient of brake pad friction material at different temperatures.

Table 2. The wear rates and friction coefficients of the brake pad pins measured at all testing temperatures.

Temperature	Specific Wear Volume [mm^3/mm] × 10^{-7}	Specific Wear Coefficients [m^2/N] × 10^{-15}	Coefficient of Friction (μ) Range
155 °C	30.7	61.2	0.4–0.6
200 °C	43.2	86.1	0.4–0.6
250 °C	65.0	130.4	0.5–0.6
300 °C	102.5	204.6	0.4–0.6

At the beginning of the test at 155 °C, the initial coefficient of friction value of the pin material was much more significant, which would have been brought about by surface abrasion from hard particles trapped in the surface. Carbon, a byproduct of phenolic resin decomposition at temperatures exceeding 200 °C, was extensively dispersed on plateaus (mainly primary plateaus). When there is sliding friction, carbon works as a lubricant, keeping the coefficient of friction steady between 0.4 and 0.6 at higher temperatures [19]. The coefficient of friction increased throughout the test until it reached a stable value at 300 °C; nevertheless, at this temperature, the brake pin material wore down more rapidly than it did at lower temperatures.

Table 2 demonstrates that, at 155 °C, the frictional coefficient varies across a tiny region in contrast to other high-temperature tests. The initial frictional coefficients at this temperature were 0.51; as the test progressed, a declining trend was seen; however, a final value of 0.59 was recorded. The frictional coefficients decreased due to wear products' compaction (sintering process) at high temperatures. The temperature exceeds 200 °C, and the frictional behaviour at 250 °C and 300 °C intensifies.

Up to 2500 m, the 250 °C and 300 °C friction curves show the same trend. The frictional behaviour of the 250 °C curves show a little drop due to some compaction of worn debris

on surfaces. Up to a high temperature of 300 °C, the coefficient of friction increases as temperature increases.

Further research was performed on the wear behaviour of GCI discs and brake pad pins at high temperatures. It is evident from Figure 4a and Table 2 that the wear rates of the disc and pin follow opposite trends. The wear rate of the disc decreases with an increase in temperature and the wear rate of the pin follows an increasing trend. Figure 4d displays the average elemental composition of wear debris on the GCI disc surface during various high-temperature friction tests. Figure 4b,c show the equivalent 3D profilometer data at 155 °C and 300 °C, respectively. The overall wear volume of the worn track on the GCI disc at various higher temperatures is shown in Figure 4a.

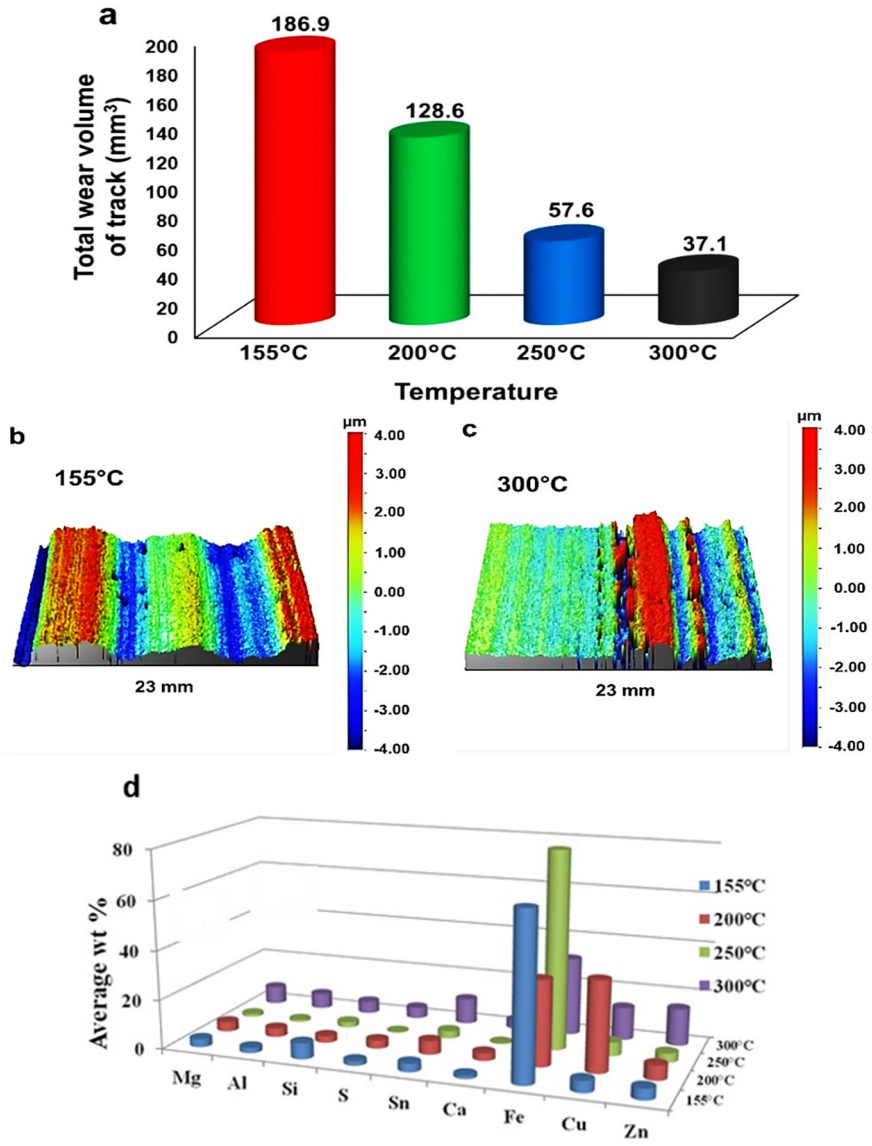

Figure 4. (**a**) Total wear volume of the worn track on the GCI disc at different elevated temperatures, (**b**,**c**) the corresponding 3D profilometer observation of the disc at 155 °C and 300 °C, and (**d**) the average elemental composition of wear debris on the GCI disc's surface, as determined using EDXS.

The abrasive Mg and Zn oxides may be the reasons why the GCI disc wore down more quickly at 155 °C (Table 1). Such oxides stimulated the counterface disc's abrasion, as seen in Figure 4b. This produced deep groves on the disc's surfaces and increased iron wt% at 155 °C (Figure 4d) compared to the results of the friction test at 300 °C. This increased iron content in the worn wear debris results from both the pin and the GCI disc.

The wear volume of the disc decreases to a significantly lower level as the temperature rises from 250 °C to 300 °C. The high temperature is strongly associated with the phenolic resin degradation of the brake pin material, resulting in loose binding properties and increasing wear particle generation from the brake pad pin (Table 2). The resin degradation also enhances the lubrication effect, with the COF values over the 300 °C friction tests being more stable and smoother (Figure 3).

The experimentally determined specific wear coefficients for the pins, as a function of disc temperature, are shown in Figure 5a. Up to a working temperature in the range of 150–200°C, the wear coefficient is initially linear, and the wear characteristics curve exhibits an exponential rise between 200 °C and 300 °C. The principle underlying a mild wear regime is that it is ruled by the production of compacted oxide layers and other alloy oxide particles on the reciprocally sliding surfaces.

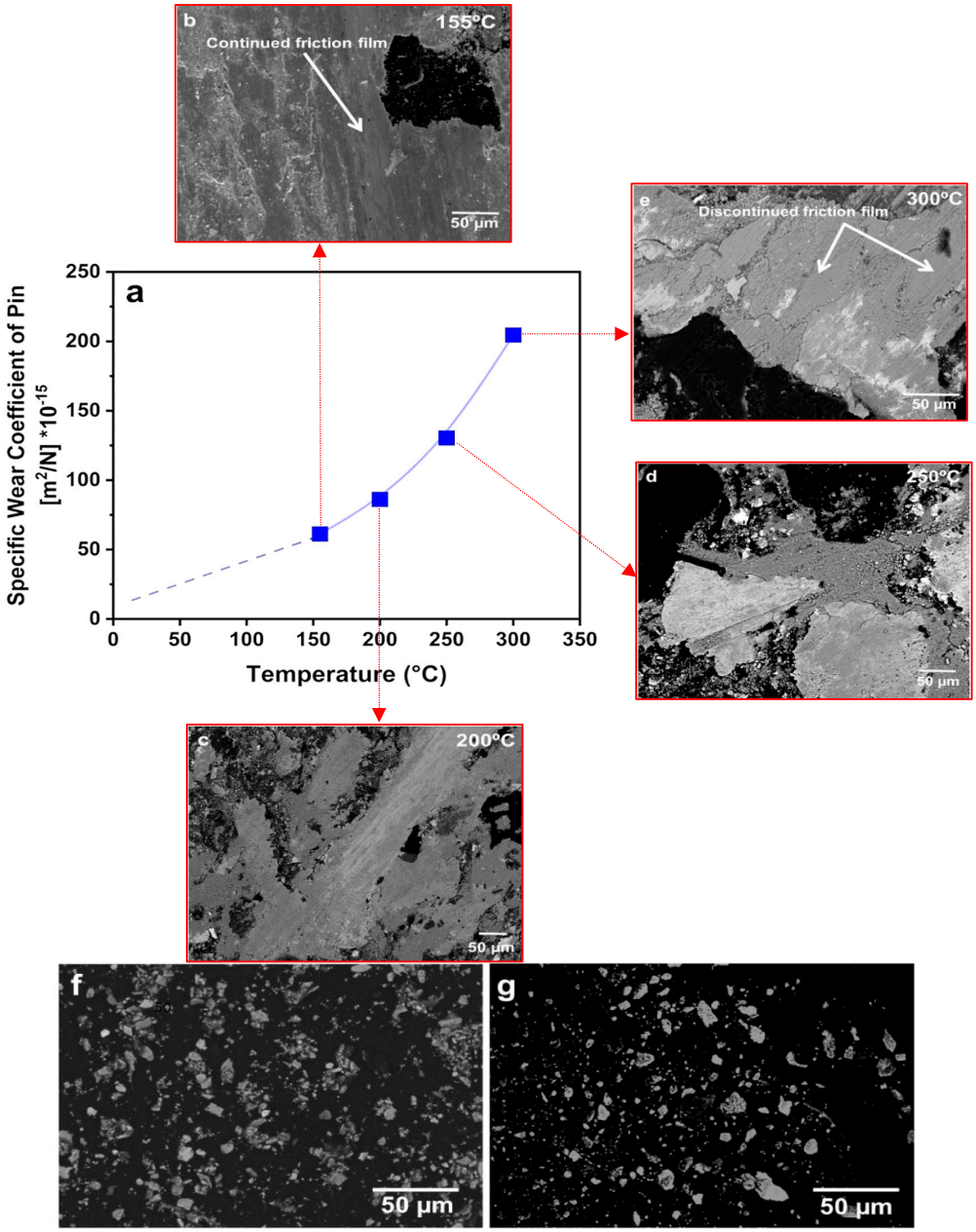

Figure 5. (**a**) Specific wear coefficients for brake pad pins in relation to disc temperature. SEM of worn surfaces of brake pad pins at different elevated temperatures: (**b**) 155 °C, (**c**) 200 °C, (**d**) 250 °C, and (**e**) 300 °C. (**f**,**g**) SEM images of loose wear debris collected at 155 °C and 300 °C friction tests.

By aggregating and compacting the wear debris produced during the sliding operation, we continued to form these layers. The friction layer, which fragmented into tiny pieces and disintegrated, contributes to the formation and release of wear particles, which become partially airborne. These compacted layers, comprising agglomerated clusters of particles subjected to thermo-elastic stresses as the sliding progressed, served as load-bearing regions or friction layers that helped to prevent the additional wear of the sliding surfaces.

Additionally, an increase in temperature accelerates sintering, which promotes the production of substantial, compacted friction layers, which reduce the wear rate. As a result, there was a mild wear region between 155 °C and 200 °C, where oxide sintering formed stable, comprehensive friction layers and reduced the specific wear rate.

The wear characteristics of the brake pins at 300 °C are demonstrated in Figure 5a, and these have a higher specific wear coefficient than those at 250 °C. It confirms that temperature significantly impacts the wear behaviour of the brake pad–disc system. The deterioration of the phenolic resins was the primary factor in the more significant specific wear coefficient at higher temperatures. Phenolic resins serve as binders in brake pad materials, holding the various components together or ensuring they were securely adhered to each other. These resins are more sensitive to high working temperatures and begin to break down at 180 °C. Higher wear rates were seen at temperatures above 200 °C because the binder started degrading, so that more wear debris was produced during the friction test.

The SEM images in Figure 5b–e show that the friction plateaus on the pin-worn surfaces. This was seen in the friction tests at 155 °C, 200 °C, 250 °C, and 300 °C. The pin-worn surfaces exhibit good coverage because the friction plateaus at 155 °C and wear debris and flakes are visible on the pin's surface. According to the EDXS results, less compacted plateaus show a significant number of Fe-rich particles, followed in terms of frequency by Zn-rich, Sn-rich, and Cu-rich particles. Primary and secondary plateaus are visible. The primary plateaus are made of mechanically stable and wear-resistant pin material components, such as the solid fibres and hard particles (see Figure 1b), which protrude from the pins' surface as they begin to wear away. Smaller wear particles tend to halt and gather at the primary plateaus, which function as obstacles to the flow of these particles [20]. Secondary plateau development is facilitated if these particles start to stick together and sinter, as observed in similar friction systems [21–24]. A negligible portion of the pin was found to have secondary plateaus as the temperature increased above 200 °C. In the relevant micrographs, only damaged primary plateaus could be seen. The coverage on the pin surface for friction plateaus is gradually reduced at higher temperatures, as shown in Figure 5d,e.

At 300 °C, deterioration and coverage with structurally disordered graphite (the black regions in Figure 5e) are widespread. This material has a refined appearance at the test temperature (as demonstrated by the friction curve in Figure 3 and confirmed by the Raman spectrum in Section 3.3, with these conditions creating a disordered graphite lattice in a temperature-dependent event). At this temperature, the residual parts of the friction plateaus can be observed and seen to be are severely damaged (Figure 5e).

The SEM images of loose wear debris collected at 155 °C and 300 °C are shown in Figure 5f,g, respectively, demonstrating the wear particle's shape and size during sliding. At 155 °C, fine wear debris was generated during the rubbing of the pin and disc. However, at 300 °C, the nature of the wear debris was coarse-grained, validating the higher wear rate data found in Table 2. Figure 5g additionally shows that this coarse wear debris does not suffer any severe fragmentation or effective grinding due to the relative sliding against the GCI disc and it is mainly released from the degradation of the phenolic resin. Therefore, temperature governs the densification of the pin material, particularly the depletion of the inorganic components, which decreases density and increases porosity.

The picture from the friction data suggests that the deterioration of the inorganic binder significantly influences the tribological characteristics of used pins at various disc

temperatures. When the inorganic binder starts to degrade, this affects the stability of the brake pin material and simultaneously releases more wear dust.

3.2. X-Ray Diffraction of the Worn Pin Surfaces

To obtain a more thorough knowledge of the wear behaviour of brake pad pins at high temperatures, X-ray diffraction was conducted on the surface of the pins after the pin-on-disc tests to determine the main phases present on the worn pin surface. All pin samples were measured via reflection geometry using a fixed incident beam (omega = 10°) to avoid collecting excessive signals from the substrate and the primary incident beam, maintaining a consistent beam penetration depth into the friction layer. Figure 6a displays the experimental X-ray diffraction data from the pin surfaces at various temperatures: 155 °C, 200 °C, 250 °C, and 300 °C.

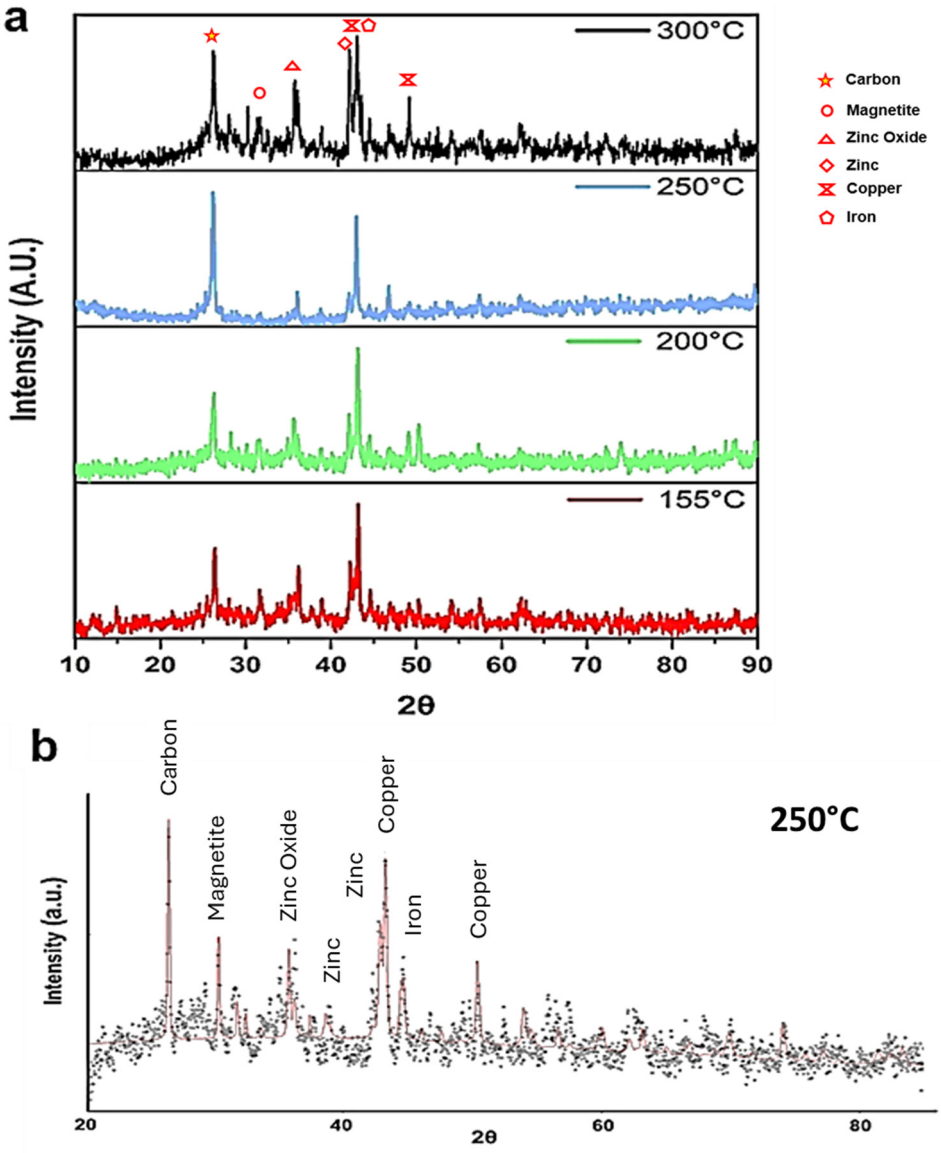

Figure 6. (**a**) Comparison of XRD spectra acquired on brake pad pin samples at 155 °C, 200 °C, 250 °C, and 300 °C, respectively. (**b**) Full-profile Rietveld fit using the MAUD software for pin samples at 250 °C.

A qualitative analysis was carried out based on the available information regarding chemical composition. Fe, Cu, Zn, Mg, and C phases were the search–match process's focus (pure elements and oxides). Working based on the qualitative findings, the full-profile

Rietveld technique was used in quantitative analysis using the MAUD program (version: 2.9994). The full-profile Rietveld fit analysis for a pin sample, performed at 250 °C using the MAUD software, is shown in Figure 6b.

Table 3 summarizes the complete quantitative analysis for all high-temperature worn pin samples. The presence of the carbon phase (graphite) as one of the principal phases in all high-temperature friction tests, primarily resulting from the degradation of the resin binder, was an interesting observation. Compared to the test at 155 °C, a 30% increase in carbon content was seen at 300 °C. The picture from the data indicates that the rise in temperature plays a crucial role in forming the decomposed carbon phase. At 300 °C, the presence of disordered graphite (a black carbonaceous byproduct) was significantly higher, leading to an anticipated double effect. When the decomposition of the inorganic components starts, as shown in Table 2, the degradation of the binder affects the binder's capacity to maintain the stability of the brake pin and releases a significant amount of wear debris.

Table 3. Results of a quantitative crystallographic investigation of a friction material pin.

Phase W%/Sample	**155 °C**	**200 °C**	**250 °C**	**300 °C**
Carbon/Graphite (C)	18.22	20.46	23.39	23.19
Iron (Fe)	0.84	0.17	0.81	0.41
Hematite (Fe_2O_3)	0.78	0.23	0.21	0.13
Magnetite (Fe_3O_4)	3.10	2.63	4.79	4.48
Zincite (ZnO)	3.03	0.32	2.53	1.13
Periclase (MgO)	6.30	3.06	11.54	5.68
Copper (Cu)	31.79	50.03	42.11	48.67
Zinc (Zn)	35.57	22.18	13.41	15.92
Tenorite (CuO)	0.37	0.92	1.21	0.39

The lower amount of Fe seen in Table 3 may result from the hard particles (MgO) removing iron plateaus. All other identified phases were already present in the brake pad material, and the wear process removed them. The primary plateaus contain copper because the copper phase is significant at various temperatures. The set of SEM microstructures on the pin surfaces in Figure 5 explicitly confirms this aspect. Understanding the considerable tribo-oxidation wear behaviour of brake pad pins at high temperatures is accomplished using X-ray diffraction (XRD).

3.3. Raman Spectroscopy

To further investigate and validate the carbonaceous breakdown products of the inorganic resin and its interfacial function at various high temperatures, Raman spectroscopy was used on the surface layer of the pin materials, as shown in Figure 7. Raman spectroscopy was employed to compare the worn-out pin surface at different working temperatures: 155 °C, 200 °C, 250 °C, and 300 °C. The finding about carbon black the presence of on the worn surfaces is very noteworthy (characteristic lines at 1360 cm^{-1} and 1590 cm^{-1}). There is a high probability of obtaining disordered graphite as the graphite is used as fibres and lubricating agents in the friction composite material for the purpose of achieving better strength and lubrication, respectively.

The disordered graphite structure (D-band) has the maximum intensity in the spectrum at 1360 cm^{-1}, whereas the polycrystalline phase of graphite (G-band) has the highest frequency at around 1590 cm^{-1} [19,20].

According to Figure 7, the oxidation reaction of the phenolic resin binder during high-temperature wear tests likely contributes to the formation of black carbonaceous

products. As the temperature rises, the resin undergoes further degradation, leading to the development of more graphitic structures.

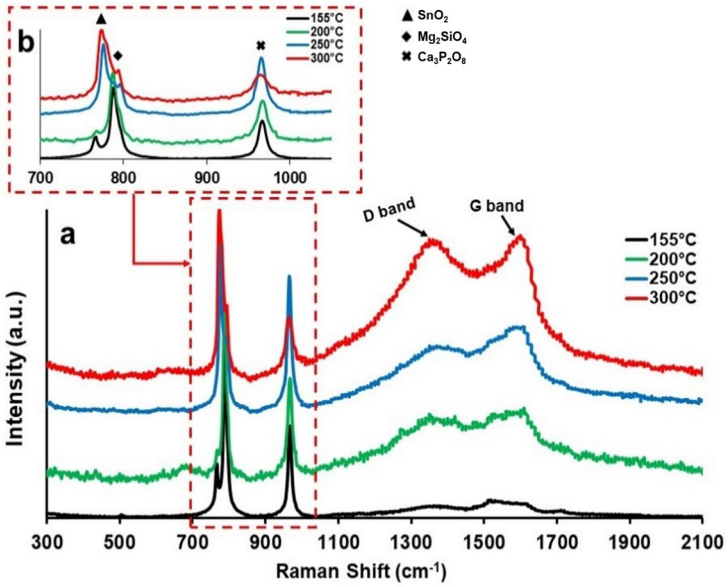

Figure 7. (**a**) A Raman spectroscopic comparison at a worn-out pin surface at various working temperatures. (**b**) A magnified image of the Raman spectra, with $Ca_3P_2O_8$ at 967 cm^{-1}, SnO_2 at 776 cm^{-1}, Mg_2SiO_4 at 790 cm^{-1}, and with ND as the corresponding wavelength.

The greater intensity of the highly disordered graphite lattice at 300 °C compared to 155 °C suggests that higher temperatures promote more extensive structural changes. This could be attributed to the enhanced thermal energy, facilitating the rearrangement of carbon atoms into more disordered graphitic forms [20]. The generation of black carbonaceous products can be attributed substantially to the strong shear strain caused by the relative sliding of the pin and disc, which facilitates the dispersion of black carbonaceous products in all directions, i.e., on the plateaus of the worn pin from the source of origin.

As a result, a mixed carbonaceous friction plateau is formed, acting as a lubricant between the contacting pair. The extent to which such phenomena may occur depends entirely on the operating temperature. Figure 3 depicts this lubricating effect, consistent with the CoF value at 300 °C. This result is also supported by XRD measurements obtained at high temperatures on the surface of a worn-out pin (carbon weight percentage, as shown in Table 3).

The Raman spectra collected at various testing temperatures were carefully analyzed through a de-convolution process employing the Lorentzian method. This approach allowed for a more nuanced interpretation of the spectral data, facilitating the identification of distinct peaks and their corresponding characteristics at each temperature. As illustrated in Figure 8, the D band in the Raman spectrum indicates a defect within the graphitic structure, arising from vibrations that occur outside the plane of the carbon layers. This band underscores the presence of disorder within the material. In contrast, the G band is linked to the in-plane vibrations of carbon–carbon bonds, specifically resulting from sp^2 hybridized orbitals. This band reflects a well-ordered graphitic structure, showcasing the resonance and symmetry characteristic of carbon atoms arranged in a hexagonal configuration [25–30]. In Figure 8a–c, the intensity of the D bands appears lower than that of the G bands, suggesting well-ordered structures. However, at 350 °C (Figure 8d), the intensities of the G and D bands seem to be comparable, indicating a more disordered arrangement. The spectral analysis provided a comprehensive de-convolution of Raman peaks associated with the D1, D2, D3, D4, and G bands for soot materials, and was performed by utilizing excitation laser energies. In this analysis, the D1, D2, and D4 bands correspond to disordered graphitic lattices of varying symmetries. The D3 band represents

amorphous carbon, and the G band is indicative of the in-plane graphitic lattice exhibiting symmetry [29].

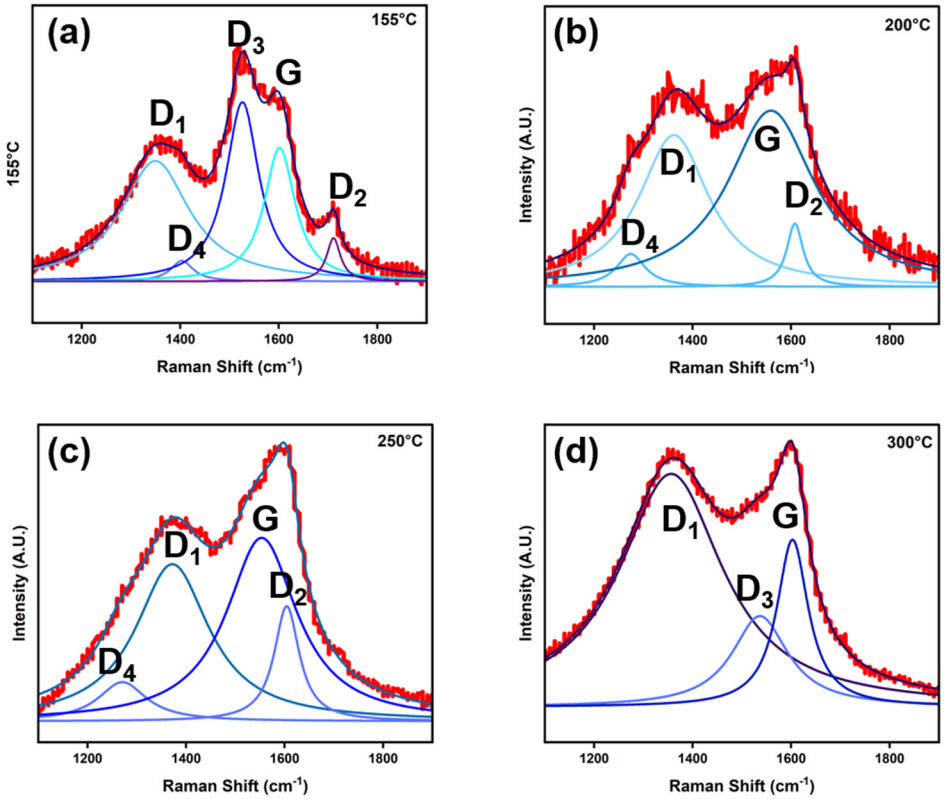

Figure 8. De-convolution of Raman spectroscopy performed on pin surface at (**a**) 155 °C, (**b**) 200 °C, (**c**) 250 °C, and (**d**) 300 °C testing temperatures.

In addition to the carbon black spectra at 1360 cm^{-1} and 1590 cm^{-1}, Figure 7 also displays additional spectra obtained from calcium phosphate, which correspond to the peak intensities at 967 cm^{-1}, SnO_2 at 776 cm^{-1}, and Mg_2SiO_4 at 790 cm^{-1} [25,26].

3.4. Wear Mechanism

The probable wear mechanisms at lower and higher temperatures, determined from the SEM-EDXS observations and analyses, are shown in Figure 9. For the lower temperature, i.e., 155 °C, the initial wear mechanism can be classified as an abrasive wear mechanism. Since the abrasive particles are held together with the complete strength of the matrix, the rubbing between the pin and disc could cause the removal of materials from both the surfaces [20], as shown in the initiation mechanism visible in Figure 9a. As the test continues, the two-body mechanism wear converts into a three-body mechanism, and the shearing of the components (especially fibres) leads to the formation of primary plateaus. The aggregation and compaction of wear debris besides the primary plateau forms the secondary plateau, as discussed in Section 2.1. The continuous uniform loading and shearing lead the wear debris to roll between the contact surfaces and become further crushed in the process, leading to fine wear debris, as shown in Figure 9a in the continuation mechanism. As for the wear mechanism at 200 °C, a similar wear mechanism takes place, with the addition of an extra secondary plateau due to the softening of the matrix resin.

At 300 °C, the wear mechanism is much more complex as there are multiple factors. For the pin, complete disintegration starts beyond 250 °C leading to cracking at the initiation of the test, as shown in Figure 9b in the initiation mechanism. During the progress of the test, the disintegration rate is increased, leading to the breaking of the matrix and the removal of the constituent particles of the brake pin. Hence, the wear rate of the disc was less

when compared with wear rates at other working temperatures. The average composition shown in Figure 4d suggests the wear debris consisted mainly of pin elements. The debris generated is coarse in nature, suggesting the absence of continuous uniform loading due to the breaking of the matrix.

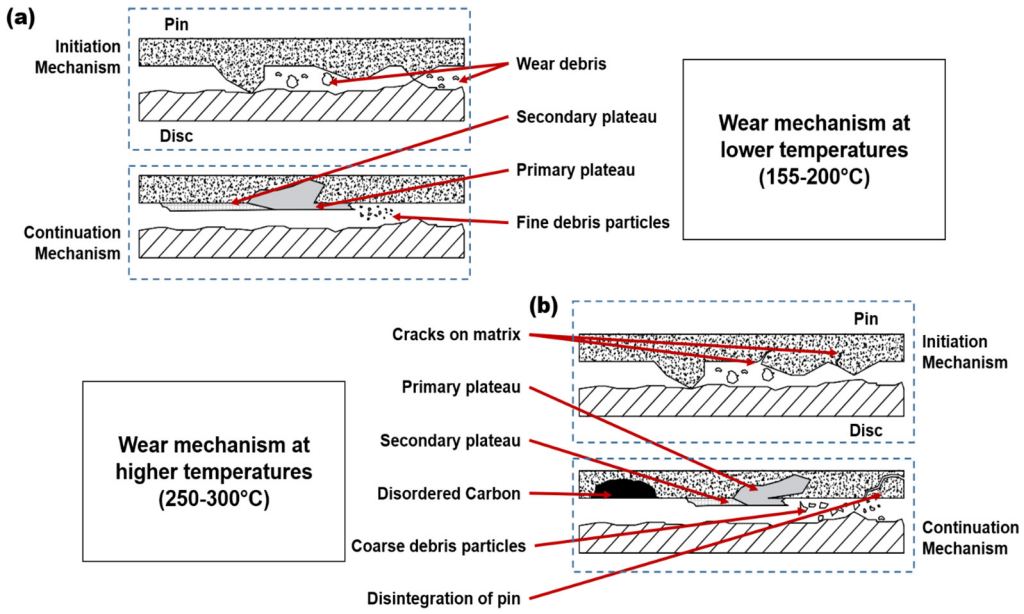

Figure 9. Wear mechanism for friction tests at (**a**) lower (155–200 °C) and (**b**) higher temperatures (250–300 °C).

Even though the primary and secondary plateaus are generated, the presence of coarse debris tend to damage them and reduce the coverage of the plateaus. However, the CoF graph is stabilized as the formation of disordered carbon due to the high temperature acts as an alternative mechanism that provides lubrication. This disordered carbon is in the form of graphite (as discussed in Section 3.3) and provides added lubrication to the brake pin–disc contact.

4. Conclusions

This research uses a high-temperature pin-on-disc tribometer to investigate the main tribological phenomena occurring when testing a commercial friction material against a cast iron slider at high temperatures. Particular interest was devoted to the carbonaceous breakdown of the inorganic binder in brake pad friction material as a function of disc temperature. The disc temperature range was maintained between 155 °C and a maximum of 300 °C to examine how the inorganic resin decomposition at high temperatures impacts the tribo pair's friction qualities. A thorough investigation was performed using experimental techniques such as X-ray diffraction, Raman spectroscopy, SEM, and EDXS. The following key conclusions can be drawn from this study:

At high temperatures (300 °C), the wear behaviour of the brake pin material turned out to be relatively higher as compared to the 155 °C friction test, regardless of the lower wear of the disc material and the substantial friction characteristics at 300 °C.

- These stable friction characteristics were associated with the carbonaceous products that provide the necessary lubrication effect. Raman spectroscopy was used to identify the main carbonaceous compounds in the friction plateaus of worn pin surfaces at high temperatures.
- The phenolic binder resin in the pin friction material degrades thermally, producing these carbonaceous byproducts. The relative sliding motion between the pin and the disc causes the carbonaceous products to spread over on plateaus on the worn pins, which considerably helps the friction curve's smooth growth.

- High temperatures govern the properties of the friction material and determine the increased wear seen at 300 °C.

Author Contributions: Conceptualization, G.S. and S.G.; Methodology, P.C.V. and S.G.; Validation, P.A., G.S. and S.G.; Formal analysis, P.C.V., P.A. and S.G.; Investigation, P.C.V., G.S. and S.G.; Resources, P.A.; Data curation, P.C.V.; Writing—original draft, P.C.V., G.S. and S.G.; Visualization, G.S. and S.G.; Supervision, G.S. and S.G.; Project administration, G.S. and S.G.; Funding acquisition, G.S. and S.G. All authors have read and agreed to the published version of the manuscript.

Funding: The research leading to these results has achieved funding from the European Union Seventh Framework Programme (FP-PEOPLE-2012-IAPP) under the Rebrake Project, Grant agreement no. 324385.

Data Availability Statement: The data presented in this study are available on request from the corresponding author.

Acknowledgments: The authors wish to thank Guido Perricone (Brembo S.p.A.) for useful discussions; Gloria Ischia and Lorena Maines for wear testing and characterization support.

Conflicts of Interest: The authors declare no conflict of interest.

References

1. Chan, D.; Stachowiak, G.W. Review of automotive brake friction materials. *Proc. Inst. Mech. Eng. Part D J. Automob. Eng.* **2004**, *218*, 953–966. [CrossRef]
2. Hulskotte, J.H.J.; Roskam, G.D.; Denier van der Gon, H.A.C. Elemental composition of current automotive braking materials and derived air emission factors. *Atmos. Environ.* **2014**, *99*, 436–445. [CrossRef]
3. Liew, K.W.; Nirmal, U. Frictional performance evaluation of newly designed brake pad materials. *Mater. Des.* **2013**, *48*, 25–33. [CrossRef]
4. Mulani, S.M.; Kumar, A.; Shaikh, H.N.E.A.; Saurabh, A.; Singh, P.K.; Verma, P.C. A review on recent development and challenges in automotive brake pad-disc system. *Mater. Today Proc.* **2022**, *56*, 447–454. [CrossRef]
5. Gurunath, P.V.; Bijwe, J. Friction and wear studies on brake-pad materials based on newly developed resin. *Wear* **2007**, *263*, 1212–1219. [CrossRef]
6. Křístková, M.; Filip, P.; Weiss, Z.; Peter, R. Influence of metals on the phenol–formaldehyde resin degradation in friction composites. *Polym. Degrad. Stab.* **2004**, *84*, 49–60. [CrossRef]
7. Kim, S.J.; Jang, H. Friction and wear of friction materials containing two different phenolic resins reinforced with aramid pulp. *Tribol. Int.* **2000**, *33*, 477–484. [CrossRef]
8. Garg, B.D.; Cadle, S.H.; Mulawa, P.A.; Groblicki, P.J.; Laroo, C.; Parr, G.A. Brake Wear Particulate Matter Emissions. *Environ. Sci. Technol.* **2000**, *34*, 4463–4469. [CrossRef]
9. Gasser, M.; Riediker, M.; Mueller, L.; Perrenoud, A.; Blank, F.; Gehr, P.; Rothen-Rutishauser, B. Toxic effects of brake wear particles on epithelial lung cells in vitro. *Part. Fibre Toxicol.* **2009**, *6*, 30. [CrossRef]
10. Perricone, G.; Alemani, M.; Metinöz, I.; Matějka, V.; Wahlström, J.; Olofsson, U. Towards the ranking of airborne particle emissions from car brakes—A system approach. *Proc. Inst. Mech. Eng. Part D J. Automob. Eng.* **2017**, *231*, 781–797. [CrossRef]
11. Kukutschová, J.; Roubíček, V.; Malachová, K.; Pavlíčková, Z.; Holuša, R.; Kubačková, J.; Mička, V.; MacCrimmon, D.; Filip, P. Wear mechanism in automotive brake materials, wear debris and its potential environmental impact. *Wear* **2009**, *267*, 807–817. [CrossRef]
12. Peikertova, P.; Filip, P. Influence of the Automotive Brake Wear Debris on the Environment—A Review of Recent Research. *SAE Int. J. Mater. Manuf.* **2016**, *9*, 133–146. [CrossRef]
13. Grigoratos, T.; Martini, G. Brake wear particle emissions: A review. *Environ. Sci. Pollut. Res.* **2015**, *22*, 2491–2504. [CrossRef] [PubMed]
14. Alves, D.D.; Riegel, R.P.; Klauck, C.R.; Ceratti, A.M.; Hansen, J.; Cansi, L.M.; Pozza, S.A.; de Quevedo, D.M.; Osório, D.M.M. Source apportionment of metallic elements in urban atmospheric particulate matter and assessment of its water-soluble fraction toxicity. *Environ. Sci. Pollut. Res.* **2020**, *27*, 12202–12214. [CrossRef]
15. Saurabh, A.; Verma, P.C.; Dhir, A.; Sikder, J.; Saravanan, P.; Tiwari, S.K.; Das, R. Enhanced tribological performance of MoS_2 and hBN-based composite friction materials: Design of tribo-pair for automotive brake pad-disc systems. *Tribol. Int.* **2024**, *199*, 110001. [CrossRef]
16. Jiang, J.; Stott, F.H.; Stack, M. The role of triboparticulates in dry sliding wear. *Tribol. Int.* **1998**, *31*, 245–256. [CrossRef]
17. Ingo, G.M.; D'Uffizi, M.; Falso, G.; Bultrini, G.; Padeletti, G. Thermal and microchemical investigation of automotive brake pad wear residues. *Thermochim. Acta* **2004**, *418*, 61–68. [CrossRef]
18. Verma, P.C.; Ciudin, R.; Bonfanti, A.; Aswath, P.; Straffelini, G.; Gialanella, S. Role of the friction layer in the high-temperature pin-on-disc study of a brake material. *Wear* **2016**, *346–347*, 56–65. [CrossRef]

19. Straffelini, G.; Verlinski, S.; Verma, P.C.; Valota, G.; Gialanella, S. Wear and Contact Temperature Evolution in Pin-on-Disc Tribotesting of Low-Metallic Friction Material Sliding Against Pearlitic Cast Iron. *Tribol. Lett.* **2016**, *62*, 36. [CrossRef]
20. Manoj, A.; Saurabh, A.; Narala, S.K.R.; Saravanan, P.; Natu, H.P.; Verma, P.C. Surface modification of grey cast iron by laser cladding for automotive brake disc application. *Wear* **2023**, *532–533*, 205099. [CrossRef]
21. Österle, W.; Urban, I. Third body formation on brake pads and rotors. *Tribol. Int.* **2006**, *39*, 401–408. [CrossRef]
22. Lutterotti, L. Total pattern fitting for the combined size–strain–stress–texture determination in thin film diffraction. *Nucl. Instrum. Methods Phys. Res. Sect. B Beam Interact. Mater. Atoms* **2010**, *268*, 334–340. [CrossRef]
23. Patel, M.; Azanza Ricardo, C.L.; Scardi, P.; Aswath, P.B. Morphology, structure and chemistry of extracted diesel soot—Part I: Transmission electron microscopy, Raman spectroscopy, X-ray photoelectron spectroscopy and synchrotron X-ray diffraction study. *Tribol. Int.* **2012**, *52*, 29–39. [CrossRef]
24. Cuesta, A.; Dhamelincourt, P.; Laureyns, J.; Martínez-Alonso, A.; Tascón, J.M.D. Raman microprobe studies on carbon materials. *Carbon* **1994**, *32*, 1523–1532. [CrossRef]
25. Li, Y.; Zhu, X.; Wang, Q.; Jiang, S.; Yang, Y.; Luo, W.; Wang, X. Apatite in *Hamipterus tianshanensis* eggshell: Advances in understanding the structure of pterosaur eggs by Raman spectroscopy. *Herit. Sci.* **2022**, *10*, 84. [CrossRef]
26. Asaithambi, S.; Sakthivel, P.; Karuppaiah, M.; Hayakawa, Y.; Loganathan, A.; Ravi, G. Improved photocatalytic performance of nanostructured SnO_2 via addition of alkaline earth metals (Ba^{2+}, Ca^{2+} and Mg^{2+}) under visible light irradiation. *Appl. Phys. A* **2020**, *126*, 265. [CrossRef]
27. Ferrari, A.C. Raman spectroscopy of graphene and graphite: Disorder, electron–phonon coupling, doping and nonadiabatic effects. *Solid State Commun.* **2007**, *143*, 47–57. [CrossRef]
28. Ferrari, A.C.; Robertson, J. Resonant Raman spectroscopy of disordered, amorphous, and diamondlike carbon. *Phys. Rev. B* **2001**, *64*, 075414. [CrossRef]
29. Zhang, C.C.; Hartlaub, S.; Petrovic, I.; Yilmaz, B. Raman spectroscopy characterization of amorphous coke generated in industrial processes. *ACS Omega* **2022**, *7*, 2565–2570. [CrossRef]
30. Parlinski, K.; Piekarz, P. Ab initio determination of Raman spectra of Mg_2SiO_4 and $Ca_2MgSi_2O_7$ showing mixed modes related to LO/TO splitting. *J. Raman Spectrosc.* **2021**, *52*, 1346–1359. [CrossRef]